

Finite size scaling for percolation on elongated lattices in two and three dimensions

S. J. Marrink

Department of Applied Mathematics, Research School of Physical Sciences and Engineering, Australian National University, Canberra, Australian Capital Territory 0200, Australia

Mark A. Knackstedt

Department of Applied Mathematics, Research School of Physical Sciences and Engineering, Australian National University, Canberra, Australian Capital Territory 0200, Australia

and School of Petroleum Engineering, University of New South Wales, Sydney, New South Wales 2052, Australia

(Received 6 December 1999)

We derive scaling laws for the percolation properties of an elongated lattice, i.e., those with dimensions of $L^{d-1} \times nL$ in d dimensions, where n denotes the aspect ratio of the lattice. Based on statistical arguments it is shown that, in the direction of the extension, the percolation threshold scales approximately as $\ln n^{1/a}$ in both two and three dimensions. Extensive Monte Carlo simulations of the site percolation model confirm this scaling behavior. It is further shown that the density of the incipient infinite cluster at the percolation threshold scales differently in two and three dimensions.

PACS number(s): 64.60.Ak, 47.55.Mh, 05.70.Jk

I. INTRODUCTION

Percolation [1] is perhaps the simplest nontrivial model in statistical mechanics. A broad array of techniques have been used to study percolation, and it has continued to be an active research area due to its relevance to a wide variety of disciplines [2–4]. In most studies of percolation theory lattices of size L^d have been used. Surprisingly, the study of percolation properties in an elongated geometry, i.e., a d -dimensional lattice of size $L^{d-1} \times nL$, has received little attention, despite the fact that in many applications one must consider such geometries. Motivated by the study of adsorption on terraced substrates, Monetti and Albano [5,6] presented a study of the finite-size effects on percolation thresholds in an elongated geometry. Other groups [7–9] have recently considered the spanning probability along elongated grids at the critical occupation probability p_c . Our interest in this problem is motivated by the common measurements of multiphase flow properties in porous media performed in the petroleum industry on rock cores of 1–5 cm in diameter and up to a meter in length [10]. Measurements on these elongated cores are used as input to reservoir simulation models. Interpretation of laboratory measurements on cores requires understanding the effect of the aspect ratio of a sample on its resultant multiphase flow process. Of particular interest is the residual or trapped fluid-phase saturations in two-phase displacements [3,11], where the amount of residual fluid is analogous to the percolation threshold p_c . Since percolation theory has been successful in providing valuable insight into two-phase flow in porous media, we consider the problem of percolation on an elongated lattice.

Using scaling arguments and small-scale numerical simulations, Monetti and Albano [5] presented scaling laws for the percolation probability in the elongated geometry that depend on the aspect ratio of the lattice. In this paper we derive new scaling laws for percolation properties of elongated lattices in both two and three dimensions, and present extensive numerical data to confirm the theoretical results.

We also define a connection probability that individual percolating clusters on square or cubic grids are connected across an intersecting surface. We consider scaling of the percolation probability, the percolation thresholds, the connection probability, the spanning probability, and the density of the percolating cluster on elongated lattices (EL).

The outline of the rest of this paper is as follows. The next section contains the theoretical derivation of scaling of the percolation threshold, the spanning probability, and the density of the incipient infinite cluster at the threshold. In Sec. III we describe the simulation methods and numerical results are presented. Comparison with the predictions of the theoretical section are also made. The conclusions are given in Sec. IV. A shorter version of this paper, comparing the scaling predictions for ordinary percolation on ELs to those obtained for invasion percolation, has been published elsewhere [12].

II. THEORY

A. Scaling of the percolation threshold: Simple lattice

Consider a d -dimensional lattice of size L^d , which we refer to as the simple lattice (SL). The expected value of its percolation threshold, $\langle p_c(L) \rangle$, depends on the size L of the system. For $L \rightarrow \infty$ numerical estimates indicate that, $\langle p_c(\infty) \rangle = 0.592\,746$ and $0.311\,608$ [9] for site percolation on the square and simple-cubic lattices, respectively. Due to the finite-size effects, the effective percolation threshold of any finite-size lattice is distributed around this expected value according to a probability distribution $F(p_c, L)$ with the expected value $\langle p_c(L) \rangle$ and a size-dependent standard deviation $\sigma(L)$.

Both $\langle p_c(L) \rangle$ and $\sigma(L)$ follow scaling laws governed by the universal scaling exponent ν

$$\langle p_c(L) \rangle - \langle p_c(\infty) \rangle \propto L^{-1/\nu} \quad (2.1)$$

and

$$\sigma(L) \propto L^{-1/\nu}, \quad (2.2)$$

where ν is the critical exponent of percolation correlation length, and $\nu=4/3$ and $\nu \approx 0.88$ in two and three dimensions, respectively [1]. The value of the proportionality factors depends on the lattice type, as well as on the definition of the percolation rule. Different rules were first considered by Reynolds *et al.* [13]; one for percolation *either* horizontally or vertically, one for a specified direction, and the third for percolation in *both* directions. As we are motivated by laboratory core measurements, we consider percolation in a specified direction—along the elongated axis.

B. Scaling of the percolation threshold: Elongated lattice

Now consider an EL consisting of nL^d SL's linked together in series. Each of the SL's percolates at a percolation threshold $p_c(L)$ according to the probability distribution $F(p_c, L)$. The percolation threshold $p_c^{(n)}(L)$ of the EL, specified along the direction of the extension, is determined by the SL with the highest percolation threshold; this lattice forms the ‘‘bottleneck’’ to percolation of the EL. The probability $P(p, L)$ of having a SL percolating at $p_c(L) < p$ is given by

$$P(p, L) = \int_0^p F(p_c, L) dp_c, \quad (2.3)$$

assuming that $F(p_c, L)$ is normalized. The probability $P_n(p, L)$ that the EL percolates at $p_c^{(n)}(L) < p$ is given by the product of n independent probabilities $P(p, L)$, i.e.,

$$P_n(p, L) = [P(p, L)]^n \times [C(p, L)]^{n-1}, \quad (2.4)$$

which is essentially an exponential decay with n , a behavior expected from the transfer matrix formulation of crossing [14]. In Eq. (2.4) $C(p, L)$ denotes the connection probability, i.e., the probability that individual percolating clusters of the SL's are mutually connected in order to form a percolating cluster across the whole EL. In the next section we will derive equations to estimate this connection probability. For the moment we assume that $C(p, L) = 1$, i.e., if each of the SL's percolate, so does the EL.

The probability distribution $F_n(p_c^{(n)}, L)$ for an EL percolating at $p_c^{(n)}(L)$ is then

$$F_n(p_c^{(n)}, L) = dP_n[p_c^{(n)}(L), L] / dp_c^{(n)}(L), \quad (2.5)$$

with the expected value $\langle p_c^{(n)}(L) \rangle$ given by

$$\langle p_c^{(n)}(L) \rangle = \int_0^1 p_c^{(n)}(L) F_n(p_c^{(n)}, L) dp_c^{(n)}(L). \quad (2.6)$$

In order to predict the scaling behavior for the percolation threshold of EL, we now assume that the percolation probability distribution $F(p_c, L)$ can be accurately described by a distribution of the form:

$$F(p_c, L) = ce^{-(x_c^a)} \quad (2.7)$$

with $x_c = [p_c(L) - \langle p_c(L) \rangle] / b$, a , b , and c being constants. With this assumption, Eq. (2.3) becomes

$$P(p, L) = bc \int_{x_0}^x e^{-(x_c^a)} dx_c \quad (2.8)$$

with $x = [p - \langle p_c(L) \rangle] / b$ and $x_0 = -\langle p_c(L) \rangle / b$. For large x , $P(p, L)$ can be approximated by

$$P(p, L) = 1 - \frac{bc}{a} x^{1-a} e^{-(x^a)} \quad (2.9)$$

Substituting this expression into Eq. (2.4) [taking $C(p, L) = 1$] we obtain

$$P_n(p, L) = \left\{ 1 - \frac{bc}{a} x^{1-a} e^{-(x^a)} \right\}^n. \quad (2.10)$$

This function approaches a Heaviside step function for large n . For one definition of a threshold, the position of the step $x[step]$ can be estimated from $P_n(p, L) = 0.5$, implying that

$$x[step] = \left\{ \ln \left(\frac{bc}{a} \right) - \ln(1 - 2^{-1/n}) + (1-a) \ln x[step] \right\}^{1/a}, \quad (2.11)$$

which, after a Taylor expansion around $1/n = 0$, gives

$$x[step] = \left\{ \ln \left(\frac{bc}{a \ln 2} \right) + \ln n + (1-a) \ln x[step] \right\}^{1/a}. \quad (2.12)$$

This equation shows that, in the limit of large n , the step takes place at large x . Therefore, the approximation leading to Eq. (2.9) is expected to be accurate. Neglecting the constants and the $\ln x$ terms [$\ln x, \ln(bc/a \ln 2) \ll \ln n$], the expression simplifies to the remarkably simple result

$$x[step] = (\ln n)^{1/a}. \quad (2.13)$$

With this result, Eq. (2.5) reduces to a delta function:

$$F_n(p_c^{(n)}, L) = \delta(x^{(n)}[step]) \quad (2.14)$$

with $x^{(n)}[step] = [p_c^{(n)}(L) - \langle p_c(L) \rangle] / b$. The equation for the expected value of the percolation threshold [Eq. (2.6)] then becomes:

$$\langle p_c^{(n)}(L) \rangle = \langle p_c(L) \rangle + b(\ln n)^{1/a}. \quad (2.15)$$

Assuming [15,16] that the distribution of percolation thresholds is approximately Gaussian [$a=2, b=\sqrt{2}\sigma(L) \propto L^{-1/\nu}$] we have

$$\langle p_c^{(n)}(L) \rangle - \langle p_c(L) \rangle \propto L^{-1/\nu} \sqrt{\ln n}. \quad (2.16)$$

However if the correlation length ξ becomes very small compared to the lattice size it has been observed numerically [15] and shown rigorously [17] that $F(p_c, L)$ is not Gaussian. Instead the distribution is characterized by $a=\nu$ and $b=L^{-1/\nu}$, which results in

$$\langle p_c^{(n)}(L) \rangle - \langle p_c(L) \rangle \propto L^{-1/\nu} (\ln n)^{1/\nu} \quad (2.17)$$

for $L \gg \xi$. Both Eqs. (2.16) and (2.17) show that the L -dependent scaling of $\langle p_c^{(n)}(L) \rangle$ for an EL will be similar to

that of an SL [Eq. (2.1)]. In the limit of $L \rightarrow \infty$, the percolation threshold for the elongated lattice will be simply $\langle p_c(\infty) \rangle$.

Due to the limiting condition that $p_c^{(n)} \leq 1.0$, the derived n -dependent scaling in Eq. (2.15) will break down for very large n or small L . A crossover towards the one-dimensional universality class should then occur, with $\langle p_c^{(n)}(L) \rangle = 1$ for $n \rightarrow \infty$. From Eq. (2.15) the aspect ratio $n_{cross}(L)$ at which this crossover occurs is expected to be

$$n_{cross}(L) = e^{(1 - \langle p_c(L) \rangle)/b)^a}. \quad (2.18)$$

It is instructive to compare the scaling relation for the percolation probability that we derived to the one derived by Monetti and Albano [5] based on scaling arguments. Their Eq. (13) can be rewritten as

$$\langle p_c^{(n)}(L) \rangle - \langle p_c(L) \rangle = c_1 L^{-1/\nu} - c_2 L^{-1/\nu} n^{-1/\nu} \quad (2.19)$$

with c_1 and c_2 denoting constants. Their equation shows the same L -dependent scaling as our derivation but a completely different n -dependent scaling [Eqs. (2.16) and (2.17)].

We also consider the critical crossing probability along the elongated axis at the critical threshold of the SL, i.e., at $p = p_c$. In two dimensions with periodic boundary conditions along the nonelongated axes, the crossing probability was given by [18] $P_n(p_c, L) \approx e^{-5n/24\pi}$. For open boundary conditions, Cardy [7] suggested $P_n(p_c, L) \approx C e^{-n\pi/3}$ with $C = 1.426348$ [8,19]. While higher-order correction terms have been evaluated for this expression [20], significant deviations from the leading exponential term occur only for n less than about 1.5. Also in three dimensions it was hypothesized [9] that an exponential form describes the crossing probability $P_n(p_c, L) \approx a e^{bn}$ and the constants were evaluated for a system with periodic boundary conditions. Using Eq. (2.4) we observe that the scaling of the percolation (crossing) probability $P_n(p_c)$ of an EL at the percolation threshold p_c of the SL in general follows this exponential form:

$$P_n(p_c, L) = P(p_c, L)^n \times C(p_c, L)^{(n-1)} = a e^{bn}, \quad (2.20)$$

where $a = C(p_c, L)^{-1}$ and $b = \ln P(p_c, L) + \ln C(p_c, L)$.

C. Connection probability

The above equations were derived using the assumption that an EL of size nL^d percolates as soon as each of the n SL's percolate. This, however, is not necessarily the case when we deal with finite size samples. The chance that the total grid percolates given that each of the SL's percolates depends on the density X^{surf} of the percolating cluster at the surfaces that form the connecting interface. Using simple statistical arguments, the chance of connection between two SL's, C_{ij} , is given by the following expression, assuming that the sites belonging to the percolating cluster are randomly distributed over the surface:

$$C_{ij} = 1 - \frac{(L^{d-1} - L^{d-1} X_i^{\text{surf}})! (L^{d-1} - L^{d-1} X_j^{\text{surf}})!}{(L^{d-1} - L^{d-1} X_i^{\text{surf}} - L^{d-1} X_j^{\text{surf}})! L^{d-1}}, \quad (2.21)$$

where X_i^{surf} and X_j^{surf} are the surface-cluster densities of the two SL's. The above formula applies to the situation when the total surface density of the two SL's is less than one, i.e., $X_i^{\text{surf}} + X_j^{\text{surf}} < 1$. In the case $X_i^{\text{surf}} + X_j^{\text{surf}} \geq 1$ the grids will always be connected, so $C_{ij} = 1$. Note that Eq. (2.21) neglects the possibility that the percolation clusters of the two SL's can still be connected on an EL via smaller clusters that traverse the connecting surfaces. Also the assumption of a random distribution of percolating surface sites is not expected to be realistic as one would rather expect a fractal distribution.

For two arbitrary SL's that are part of an EL, the surface densities X_i^{surf} and X_j^{surf} obey a probability distribution that depends on the value of p_n , which we denote $F^{\text{surf}}(X^{\text{surf}}, p, L)$. The connection probability for two of these SL's is given by

$$C(p, L) = \int_0^1 F^{\text{surf}}(X^{\text{surf}}, p, L) \times \int_0^1 F^{\text{surf}}(X^{\text{surf}}, p, L) C_{ij} dX_i^{\text{surf}} dX_j^{\text{surf}} \quad (2.22)$$

The functional form of $F^{\text{surf}}(X^{\text{surf}}, p, L)$ is not straightforward to predict, however. In the results section we will try to evaluate this distribution using the following expression:

$$F^{\text{surf}}(X^{\text{surf}}, p, L) = \int_0^p F(p_c, L) F_c^{\text{surf}}(X^{\text{surf}}, p, p_c, L) dp_c, \quad (2.23)$$

where $F_c^{\text{surf}}(X^{\text{surf}}, p, p_c, L)$ is the surface density distribution for an SL with occupation density p and percolation threshold p_c . $F(p_c, L)$ is the probability for an SL to percolate at threshold p_c . For large n , the distribution $F^{\text{surf}}(X^{\text{surf}}, p, L)$ is expected to approach the true distribution of surface densities in an EL.

To give insight into the scaling of the connection probability, we make the following further assumptions. First assume that the surface density distributions are delta functions, corresponding to the expectation value of the distribution. We now have $F^{\text{surf}}(X_i^{\text{surf}}, p, L) = F^{\text{surf}}(X_j^{\text{surf}}, p, L) = \delta(\langle X^{\text{surf}} \rangle)$. Second, approximate Eq. (2.21) by the formula, using $n!/(n-c)! \approx (n-c/2)^c$:

$$C_{ij} = 1 - \left(1 - \frac{X_i^{\text{surf}}}{1 - X_j^{\text{surf}}/2} \right)^{X_j^{\text{surf}} L^{d-1}}. \quad (2.24)$$

Together with the first approximation we have

$$C(p, L) = 1 - \left(1 - \frac{\langle X^{\text{surf}} \rangle}{1 - \langle X^{\text{surf}} \rangle/2} \right)^{\langle X^{\text{surf}} \rangle L^{d-1}}, \quad (2.25)$$

which equals

$$C(p, L) = 1 - e^{(-L^{d-1} \langle X^{\text{surf}} \rangle^2)} \quad (2.26)$$

to first-order expansion of $\ln[1 - \langle X^{\text{surf}} \rangle / (1 - \langle X^{\text{surf}} \rangle / 2)]$, which is accurate for $\langle X^{\text{surf}} \rangle \ll 0.5$. We recall that for $\langle X^{\text{surf}} \rangle \geq 0.5$, $C(p, L) = 1$.

The extent to which the approximations we have made are valid will become clear in the results section, where we compare the connection probability curves calculated according to Eqs. (2.22), (2.25), and (2.26) to the connection probability curve derived from simulation results for the EL and the use of Eq. (2.4):

$$C(p, L) = \left\{ \frac{P_n(p, L)}{[P(p, L)]^n} \right\}^{1/(n-1)}. \quad (2.27)$$

The evaluation of $C(p, L)$ using this expression is expected to be independent of n .

D. Scaling of percolation density

The density of the sample-spanning cluster is the probability at p_c that a given site belongs to the percolating cluster. Considering the n SL's of the EL independently, then the local density X of the percolating cluster in each of the SL's depends both on the value of the percolation threshold $p_c^{(n)}(L)$ of the EL and on the percolation threshold $p_c(L)$ of the SL. From random percolation on SL's we can distinguish three regimes:

$$X \propto L^{-\beta/\nu} \quad [p_c^{(n)}(L) = p_c(L)], \quad (2.28)$$

$$X \propto [p_c^{(n)}(L) - p_c]^\beta \quad [p_c^{(n)}(L) > p_c(L)], \quad (2.29)$$

$$X \propto p_c^{(n)}(L) \quad [p_c^{(n)}(L) \gg p_c(L)], \quad (2.30)$$

where $\beta = 5/36$ and 0.41 in two and three dimensions, respectively. As shown in the previous section, $p_c^{(n)}(L)$ is expected to be larger than $p_c(L)$, so that all the SL's other than the ‘‘bottleneck’’ lattice are above their percolation threshold. Therefore, the densities of the individual SL's are expected to scale according to either Eqs. (2.29) or (2.30). Only the bottleneck SL scales according to Eq. (2.28).

For small n , or large L , $p_c^{(n)}(L)$ is still close to $p_c(L)$ and we expect most SL's to follow Eq. (2.29). In this case the density of the EL $X^{(n)}(L)$ scales analogously:

$$X^{(n)}(L) \propto [p_c^{(n)}(L) - p_c(L)]^\beta \quad [\text{small } n; \text{ large } L]. \quad (2.31)$$

Substituting the scaling law for $p_c^{(n)}(L)$ from Eq. (2.15) we obtain

$$X^{(n)}(L) \propto L^{-\beta/\nu} (\ln n)^{\beta/a} \quad [\text{small } n; \text{ large } L]. \quad (2.32)$$

This equation shows that the L -dependent scaling of the density of the percolating cluster of an EL is similar to a SL [cf. Eq. (2.28)]. The n -dependent scaling of the percolation density is distinct from that of the percolation threshold. In the limit of large n , a large number of the SL's enter the scaling region of Eq. (2.30), leading to a scaling prediction for the density of the elongated lattice in this limit:

$$X^{(n)}(L) = p_c^{(n)}(L) \quad [\text{large } n; \text{ small } L] \quad (2.33)$$

and using Eq. (2.15)

$$X^{(n)}(L) - p_c(L) \propto L^{-1/\nu} (\ln n)^{1/a} \quad [\text{large } n; \text{ small } L]. \quad (2.34)$$

In this case, the L -dependent scaling of the EL is different from that of a SL and the exponent β no longer appears in the scaling law.

III. NUMERICAL RESULTS AND DISCUSSION

A. Details of the simulations

The numerical results that we present are all obtained using random site percolation on a square two-dimensional (2D) and simple cubic (3D) lattice with open boundary conditions. We consider the lattice to be percolating as soon as a cluster spans it in the direction of the extension regardless of percolation in the other direction(s) (rule R_1 in the terminology of Reynolds *et al.* [13]). The percolation threshold is defined in this paper as the average value of p of the percolating (crossing) configurations defined along the extended direction. While this is one of many possible definitions [21–23] we expect that the precise definition will not affect the scaling behavior shown in this paper. The number of realizations per lattice size depends on its dimension—in general the number of realizations was chosen to obtain $p_c^{(n)}(L)$ and $X^{(n)}(L)$ to within a standard error of 0.0001 and 0.001, respectively. As an example, for a small 2D lattice of size $L = 32$ and aspect ratio $n = 4$, 250 000 independent realizations were required, whereas for a large 3D lattice of size $L = 80$ and aspect ratio $n = 10$, 200 realizations proved sufficient. In all the figures the standard error of the results is never larger than the size of the data points. More extensive computations were performed, especially in 3D, to obtain accurate predictions of the percolation and connectivity probabilities of the EL at the percolation threshold p_c of the SL.

In order to get an accurate prediction of the connection probability based on Eqs. (2.22) and (2.23), we have computed the surface density distribution $F^{\text{surf}}(X^{\text{surf}}, p, L)$ from percolation results of a SL. Random grids were generated with a percolation threshold p_c following the probability distribution $F(p_c)$. For each grid the surface density X^{surf} was evaluated for $p_c < p < 1$, i.e., all possible densities larger than the percolation density, and binned to obtain $F_c^{\text{surf}}(X^{\text{surf}}, p, p_c, L)$. The integral of Eq. (2.23) was then solved numerically to obtain $F^{\text{surf}}(X^{\text{surf}}, p, L)$. These distributions were then used to generate random pairs of surfaces, for which the connection criterion was tested. The average connection probability obtained with this Monte Carlo approach corresponds to $C(p, L)$. Note that the surface density X^{surf} of an SL differs from the average density X of the percolating cluster when using open boundary conditions.

B. Connection probability

In Figs. 1(a) (2D) and 1(b) (3D) we verify that the connection probability we compute from our numerical results according to Eq. (2.27) is indeed n independent. Curves computed for small n values have higher accuracy at low values of p , whereas large n values give higher accuracy towards larger values of p . Within the uncertainty of the results, all curves coincide for all of the L values studied.

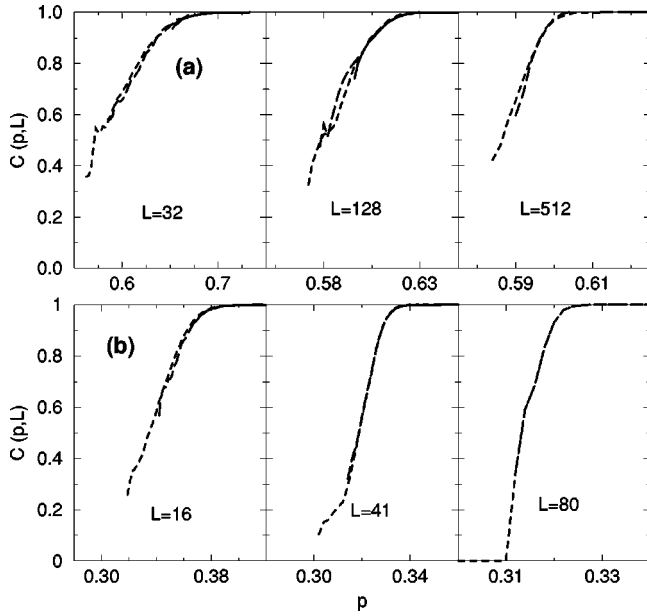


FIG. 1. Connection probabilities for EL's with different aspect ratios. Connection probabilities $C(p,L)$ are calculated according to Eq. (2.27). (a) $D=2$, with $n=2$ (dotted lines), $n=4$ (dashed lines), and $n=100$, ($L=32$), and $n=10$, ($L=128$) (solid lines). (b) $D=3$, with $n=2$ (dotted lines), $n=4$ (dashed lines), and $n=10$ (solid lines, $L=16,41$ only).

In Figs. 2(a) (2D) and 2(b) (3D) the connection probabilities derived from the simulation and use of Eq. (2.27) are plotted for three values of L , and compared to the approximated solutions, Eqs. (2.22) and (2.26), based on the measurement of the surface densities of the SL. In almost all cases the approximation of Eq. (2.25) by Eq. (2.26) is accurate so we only show Eq. (2.26). The use of Eq. (2.26), which is based on the average surface densities, slightly overestimates the connection probability compared to the more realistic approach of Eq. (2.22) which takes into ac-

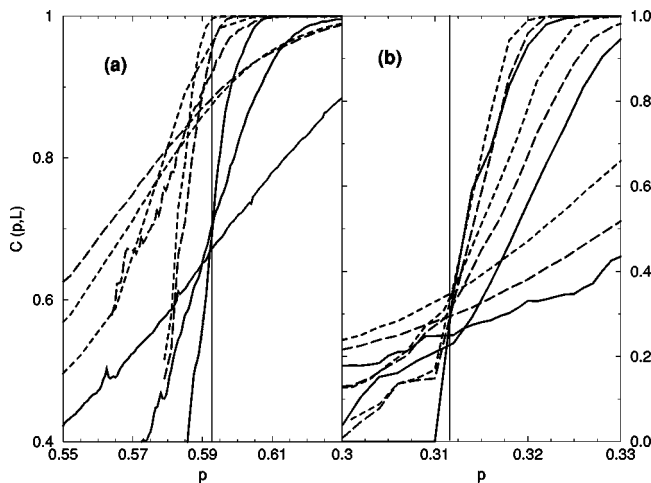


FIG. 2. Realized and predicted connection probability for EL's. Comparison of connection probability $C(p,L)$ computed according to Eq. (2.26) (short-dashed lines), Eq. (2.22) (long-dashed lines), and derived from simulation using Eq. (2.27) (solid lines). (a) $D=2$, $L=32, 128$, and 512 . (b) $D=3$, $L=16, 41$, and 80 . The steepest curves correspond to the biggest lattice size. The vertical line indicates the position of the percolation threshold of the SL.

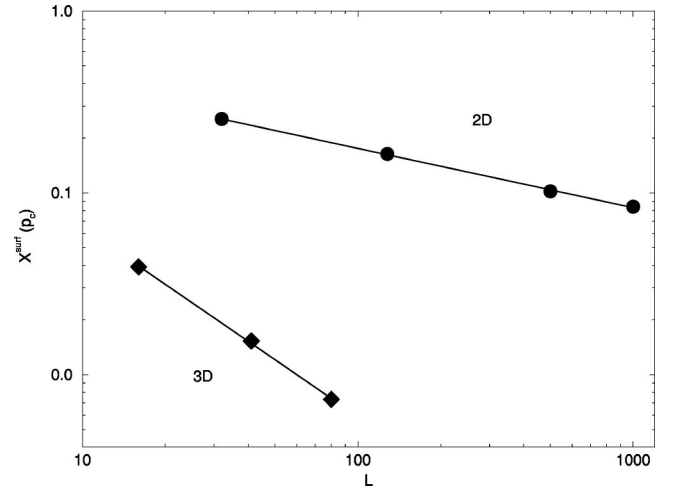


FIG. 3. L -dependent scaling of the surface density of the SL. Double-logarithmic plot of the surface density X^{surf} of the SL evaluated at p_c versus lattice size L . The solid lines indicate linear fits to the data points.

count the full distributions. Results in 3D show that Eq. (2.22) correctly predicts the simulated connection probability, especially at large L . In 2D this is not the case. The difference in 2D probably originates from our assumption of a homogeneously distributed surface density X^{surf} when calculating the connection probability according to Eq. (2.22). A fractal distribution seems more appropriate. Moreover, due to the use of open boundary conditions, the true distribution of the surface density across the connecting interface is expected to be lower along the boundaries than in the bulk. Another possible explanation for the remaining discrepancy between approximated and observed connection probabilities is the occurrence of loops that would tend to make the apparent connection probability in the EL lower. Either of these effects seem smaller in 3D than in 2D.

We note the near coincidence of the connection probability curves at the percolation threshold of the SL. In 3D, but not in 2D, the fixed point also occurs in the set of curves based on the average surface densities [Eqs. (2.22) and (2.26)]. We again attribute the discrepancy in 2D to either the assumption of a homogeneously distributed surface density or to the contribution of loops. Using Eq. (2.26) the fixed point implies that the average surface density at the fixed point scales as $X^{\text{surf}}(p_c) \propto L^{-(d-1)/2}$. Verification of this scaling relation is made in Fig. 3, which shows a log-log plot of $X^{\text{surf}}(p_c)$ vs L . Straight lines are observed both in 2D and in 3D. The slope in 3D equals -1.0 , in accordance to the anticipated slope of -1 . In 2D we find a slope of -0.33 , which indeed implies a small remaining L dependency of the connection probability at p_c computed according to Eqs. (2.25) and (2.26). The reason for the exponent of -0.33 in 2D remains unclear.

C. Connection probability vs percolation probability of SL

In Figs. 4(a) (2D) and 4(b) (3D) we compare the connection probability $C(p,L)$, i.e., the probability that the percolating cluster of two SL's are connected at the interface, to the percolation probability of the SL. It appears that both probability curves are very similar, which is an unanticipated

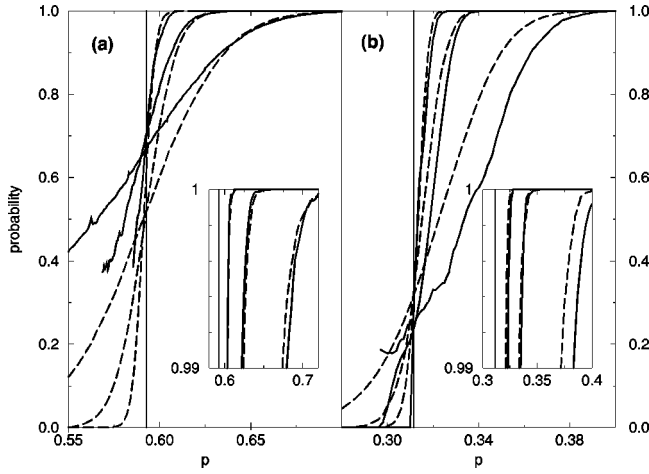


FIG. 4. Comparison of the percolation probability $P(p, L)$ of a SL (dashed lines) and the connection probability $C(p, L)$ computed according to Eq. (2.27) with $n=2$ (solid lines). (a) $D=2$, $L=32$, 128, and 512, and (b) $D=3$, $L=16$, 41, and 80. The steepest curves correspond to the biggest lattice size. The inserts show the almost identical behavior of the percolation and connection probability for $p > p_c$. Inset in (a) shows $n=100$, 10, and 4 for $L=32$, 128, and 512, and in (b) gives $n=10$, 10, and 4 for $L=16$, 41, and 80-respectively. The vertical line indicates the position of the percolation threshold of the SL.

result. Intuitively one might expect that, at a given occupation density p , it is much easier to connect two percolating interfaces rather than connect L subsequent interfaces. However, the probability of connecting any two interfaces depends on the occupation fraction p , which is much higher than the probability of connecting two percolating clusters at an interface that depends on the surface density X^{surf} of the percolating cluster. On the square lattice with open boundary conditions we obtain $P(p_c, L) \approx 0.50$, while the fixed point of the connection probability $C(p_c, L) \approx 0.68$ is significantly higher. In 3D the fixed point of the connection probability $C(p_c, L) \approx 0.23$ almost coincides with the fixed point of the percolation probability $P(p_c, L) = 0.286$. The observation of the fixed point of the percolation probability is consistent with results on the square lattice [21] and recent results based on extensive simulations on a cubic lattice [23].

For values of p much larger than p_c (see insets of Fig. 4) the connection probability and the percolation probability become indistinguishable, except for the smallest L value studied, where the coarseness of the grid becomes important. The underlying reason for the similarity between $P(p, L)$ and $C(p, L)$ remains unclear to the authors, but it allows us to simplify Eq. (2.4). Setting $C(p, L) = P(p, L)$ we obtain

$$P_n(p, L) = [P(p, L)]^{2n-1}, \quad (3.1)$$

which we expect to be especially accurate in 3D and in 2D for large values of n where $p_c^{(n)}(L) \gg p_c(L)$. Another way of interpreting Eq. (3.1) is by considering the EL to be constructed of $2n-1$ partially overlapping SL's, requiring each of them to percolate. The probability that the percolating clusters of two SL's with a 50% overlap are connected is much higher, so if each of the $2n-1$ individual SL's percolate, so does the EL. Following the same derivation as before, but now using Eq. (3.1) instead of Eq. (2.4), we have

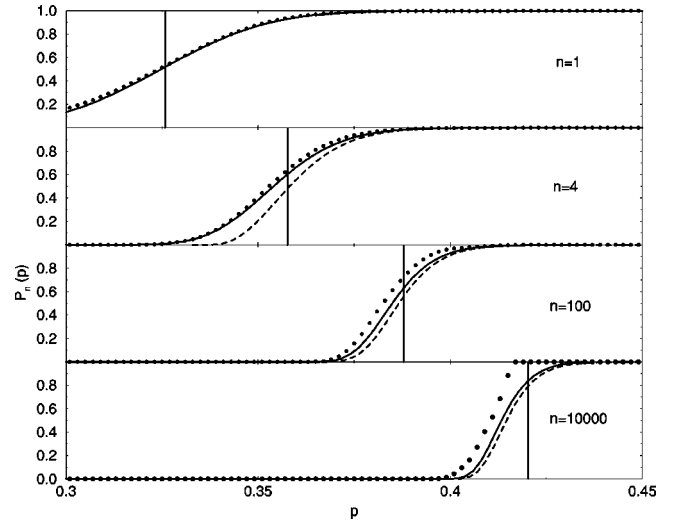


FIG. 5. Comparison of theoretical predictions for the percolation probability of EL's. Example for lattice of size $16 \times 16 \times 16n$. Four levels of approximation are shown: points: first level [application of Eq. (3.1) using simulated percolation distribution of the SL]; solid curve: second level [application of Eq. (3.1) using Gaussian fit to percolation distribution of the SL]; dashed curve: third level [application of Eq. (3.2)]; vertical lines: fourth level [approximation by Heaviside step function according to Eq. (2.13)].

$$P_n(p, L) = \left\{ 1 - \frac{bc}{a} x^{(1-a)} e^{-(x^a)} \right\}^{(2n-1)} \quad (3.2)$$

leading to only a small modification of Eq. (2.12):

$$x[\text{step}] = \left\{ \ln \left(\frac{2bc}{a \ln 2} \right) + \ln \left(n - \frac{1}{2} \right) + (1-a) \ln x[\text{step}] \right\}^{1/a}, \quad (3.3)$$

which still equals Eq. (2.13) in its simplified form ($n \gg \frac{1}{2}$).

D. Percolation probability distributions of EL's

We now compare the different theoretical approximations used to describe the percolation probability function $P_n(p, L)$ for the EL. In Fig. 5 $P_n(p, L)$, the probability that an EL percolates at $p_c^{(n)}(L) < p$, is shown for $n=1, 4, 100$, and 10000, where four curves are compared. One curve is the prediction based on directly applying Eq. (3.1) to the numerically-realized percolation threshold distribution $F(p_c, L)$ of the SL. A second curve approximates the percolation threshold distribution F by a Gaussian according to Eq. (2.7) ($a=2$), before applying Eq. (3.1). The third curve is based on Eq. (3.2), while the fourth curve gives the probability defined by a Heaviside step function at the position given by Eq. (2.13) (with $a=2$). Figure 5 shows that the approximation of the probability curves by Eq. (3.2) yields very accurate results for all n . The approximation of the position of the step by Eq. (2.13) deviates from the position for which $P_n(p, L) = 0.5$ only at very high n (10^4 in this case). This deviation originates from neglecting the $\ln x$ term in Eq. (2.13).

For extremely large n , the second curve based on a Gaussian percolation probability distribution deviates significantly from the prediction based on directly applying Eq. (3.1) to

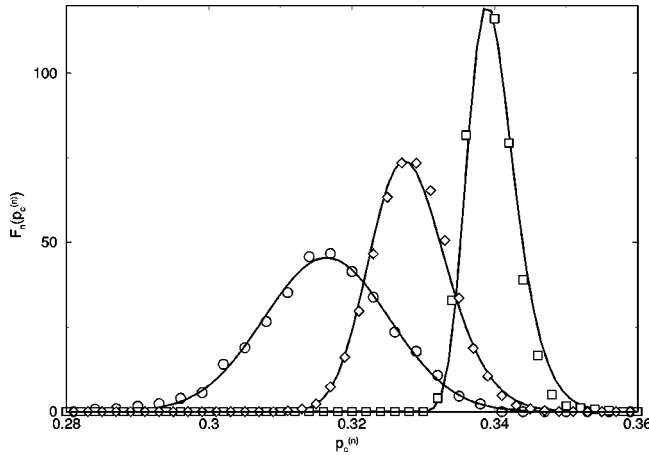


FIG. 6. Comparison of theoretically predicted and simulated percolation probability distributions. Example for lattices of size $41 \times 41 \times 41n$. Open symbols are used for simulated percolation probability distributions for the SL (circles), and for EL's with $n = 4$ (diamonds), and $n = 100$ (squares). Solid lines are theoretical predictions based on approximating $F(p_c, L)$ by a Gaussian and applying Eq. (3.1).

the numerical distribution. For large n the percolation probability $P_n(p, L)$ is determined by the tail of the distribution, $P(p, L) \rightarrow 1.0$, of the SL. Due to the numerical noise and the limited accuracy of the numerical distribution for the SL at $p \gg p_c$, we believe that the Gaussian fit captures this tail without the numerical noise, and therefore gives a better fit for larger n . We show in Fig. 6 that the assumption of a Gaussian distribution gives an excellent match to the numerical data obtained at large n . Figure 6 displays as an example the numerically obtained percolation probability distribution F_n for a 3D lattice of size $41 \times 41 \times 41n$ plus the predictions based on Eq. (2.5) and Eq. (3.1) using a Gaussian fit to the percolation probability distribution F of the SL. F_n was obtained from P_n as a numerical derivative, as there is no analytical expression for F_n . As we will see when we present the full n -dependent scaling results of both 2D and 3D percolation thresholds, the assumption of a Gaussian distribution for the SL fits the 3D data only. One should realize that, even in 3D, the percolation probability distributions of an EL are not Gaussian. As can be seen from Fig. 6 the probability distributions are skewed.

E. L -dependent scaling of percolation threshold of EL

In Fig. 7(a) we show numerical results obtained on 2D lattices with size L ranging from 16 to 2048 and aspect ratios $1 < n \leq 10^3$. Independent of n , all the curves follow the same scaling law over a broad range of L , confirming the L -dependent scaling of the percolation threshold of an EL as given by Eqs. (2.16) and (2.17). The straight lines are linear fits to all the data points, except for those for $L = 16$, which seem to be consistently smaller. As in site percolation on SL's in the limit of small L , the scaling relations may breakdown. For $L \rightarrow \infty$, all the curves extrapolate to a percolation threshold very close to that of a SL. Any difference disappears if the fit is based on progressively higher values of L for larger values of n . Figure 7(b) shows the results obtained

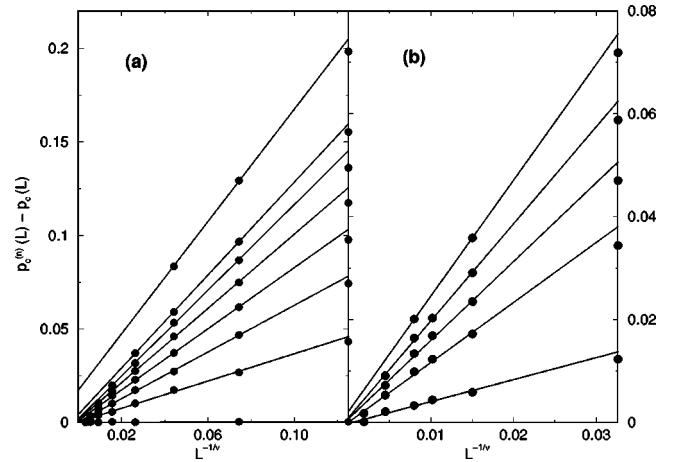


FIG. 7. L -dependent scaling of the percolation threshold for EL's. Points represent numerical data, and solid lines linear fits to the data excluding the smallest L value. (a) $D = 2$, from bottom to top, $n = 1, 2, 4, 8, 16, 32, 64$, and 1000. (b) $D = 3$, $n = 1, 2, 4, 10$, and 50.

with 3D lattices with $16 < L < 80$ and $1 < n < 50$. Again, the scaling is consistent with our predictions.

F. n -dependent scaling of percolation threshold of EL

The n -dependent scaling of the percolation thresholds is summarized in Fig. 8. The data are shown as $\ln n$ versus $p_c^{(n)} - p_c$ on a log-log scale. As anticipated by the theoretical analysis in the previous section, the data appear as straight lines with a slope equalling $1/a$. Leaving out the largest n values, we find that the slope of the curves equals 0.72 ± 0.05 in 2D, and 0.50 ± 0.02 in 3D, without any obvious L dependency. Comparing these results to the anticipated slopes of $1/2$ [Eq. (2.16)] and $1/\nu$ [Eq. (2.17)] reveals that the 2D data scale according to Eq. (2.17) ($1/\nu = 0.75$) whereas the 3D data scale according to Eq. (2.16). Apparently, for the

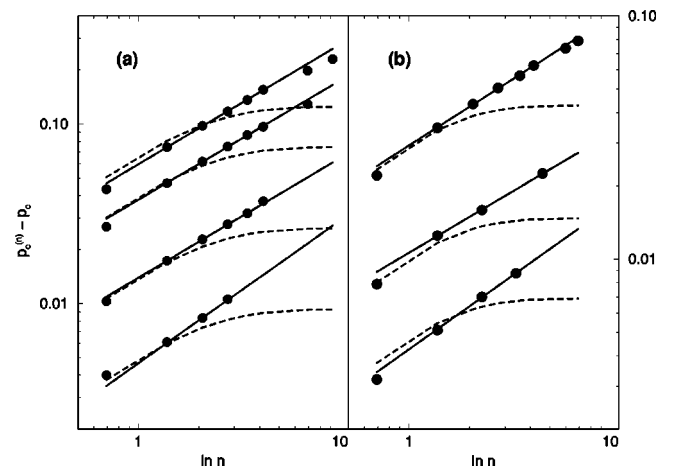


FIG. 8. n -dependent scaling of the percolation threshold of EL's. Data are shown on a log-log scale. Points represent actual percolation results for EL's and solid lines are linear fits to these results excluding, for small L , the smallest and the largest n values. (a) $D = 2$, $L = 16, 32, 128$, and 512 from top to bottom, and (b) $D = 3$, $L = 16, 41$, and 80. The dotted lines give the prediction of Monetti and Albano [Eq. (2.19), with $c_1 = c_2 = 1.0$].

2D case the correlation length drops rapidly upon extension of the lattice and scaling is determined by the tails of the percolation distribution that follow a non-Gaussian decay characterized by the correlation length exponent ν . On the contrary, in 3D the correlation length remains large and the scaling is according to a Gaussian distribution of percolation thresholds.

We do note that the scaling observed here describes neither the limiting behavior in the small n or the large n limit but describes a crossover behavior for intermediate n . For small n the approximation leading to Eq. (2.9) breaks down. For large n the theoretical predictions overestimate the numerical values, due to the neglect of the $\ln x$ term in Eq. (2.13). Numerical estimates indicate an overestimation of about 10% at $n=10^5$. A crossover to one-dimensional behavior is not observed for finite n considered here. There is no indication in the 2D data of Fig. 8 of a crossover to the one-dimensional universality class ($\nu=1$). Substituting the numerical values of a, b , and $p_c(L)$ into Eq. (2.18) reveals that the crossover may be expected to occur at extremely large n . For example, $n_{c_{ross}}(L) = O(10^{12})$ for a 2D lattice of size $L=32$, and $n_{c_{ross}}(L) = O(10^{200})$ for a 3D lattice of size $L=16$.

Except for small aspect ratios ($n < 8$) we find a significantly different n -dependent scaling of the percolation probability than conjectured by Monetti and Albano [5] (see Fig. 8). Our numerical results for larger values of n very closely match the $(\ln n)^{1/a}$ -type scaling we derived from our theoretical arguments, and certainly not the $n^{-1/\nu}$ type of scaling proposed by Monetti and Albano [5]. These authors also presented limited numerical results that seemed to confirm their scaling law. Only 2D results were reported, with small aspect ratios $n=2, 4, 8$, and 16 only, and very small lattice sizes ranging from $L=6$ to 48. Fitting of our data to their proposed scaling [Eq. (2.19)] we indeed find a good match for small n ($n < 8$), with the nontrivial result $c_1 = c_2 = 1.0$ in both 2D and 3D. However, the more extensive data set leads to large systematic deviations from their proposed scaling law. Therefore we conclude that Eq. (2.19) only holds in the limiting case of small aspect ratio. At larger values a crossover to $\ln n^{1/a}$ -type scaling occurs.

G. n -dependent scaling of percolation probability of EL at p_c

Figure 9 shows a logarithmic plot of $P_n(p_c, L)$ vs n showing straight lines in both two and three dimensions, in accordance with Eq. (2.20). Within the error bars (reflected by the size of the data points), the results are independent of L . From the slope and intercept we calculate $a=1.5$, and $b=-1.10$ in 2D, implying $P(p_c, L)=0.50$ and $C(p_c, L)=0.67$, consistent with our earlier results and with the prediction of [19], $a=1.42635$ and $b=-\pi/3=-1.05$. In three dimensions we find $a=4.5$ and $b=-2.7$, implying $P(p_c, L)=0.286$ and $C(p_c, L)=0.23$, also in agreement with our earlier results. The 3D results for $P(p_c, L)$ are similar to the recent predictions of Lin *et al.* [24] $P(p_c, L)=0.265$ and Gimel *et al.* [23] $P(p_c, L)=0.28$. The values for a and b are very different from those given by Lorenz and Ziff [9] who obtain $a=1.45$ and $b=-1.37$ for a cubic grid with periodic boundary conditions in each $L \times L$ plane. The latter result predicts that the crossing probability at p_c de-

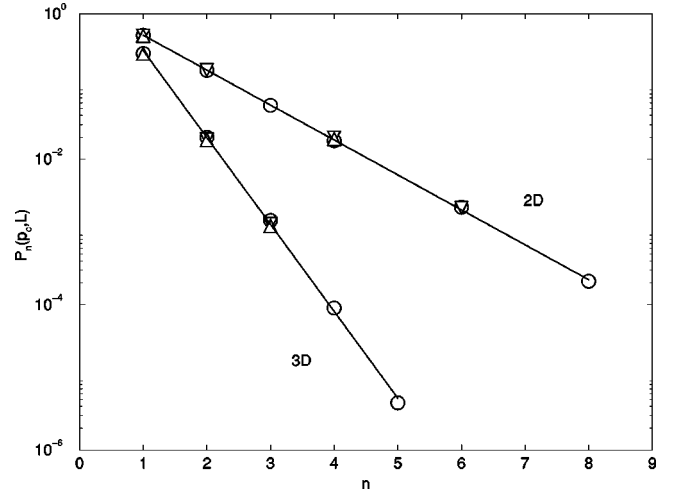


FIG. 9. n -dependent scaling of the percolation probability of an EL at p_c . Logarithmic plot of $P_n(p_c, L)$, the percolation probability of an EL at the percolation threshold of the SL vs n . Two-dimensional results are given for $L=32$ (circles), $L=128$ (triangles down), and $L=512$ (triangles up), and three-dimensional results for $L=16$ (circles), $L=30$ (triangles down), and $L=41$ (triangles up). Solid lines are linear fits to all data points.

creases by a factor $e^{-b} \approx 0.254$ for each additional cube added to an $L^2 \times nL$ lattice with periodic boundary conditions. The current paper gives $e^{-b} \approx 0.105$. This result highlights the effect of the choice of boundary condition [25] on the spanning probability.

Both 2D and 3D findings indicate that the connection probability at p_c remains finite, even in the limit of large L . Furthermore, in 3D it appears that the connection probability is smaller than the percolation probability itself.

H. L -dependent scaling of density of EL

Figures 10(a) (in 2D) and 10(b) (in 3D) show the L -dependent scaling of the density in elongated lattices. In the 3D case the scaling is in accordance with Eq. (2.32) over the entire ranges of L and n studied. Apparently, the percolation threshold $p_c^{(n)}(L)$ of the EL is still close enough to the individual percolation thresholds $p_c(L)$ of the SL's, so the contribution of SL's scaling according to Eq. (2.34) remains negligible. In 2D, this is only true for large L and small n . As L decreases, or n increases, the curves do approach the limiting scaling law, Eq. (2.33).

I. n -dependent scaling of density of EL

Figures 11(a) and 11(b) present the n -dependent scaling behavior of the percolation density. As was concluded from the L -dependent scaling in the previous section, in the 3D case [Fig. 11(b)] the scaling relation given by Eq. (2.32) holds well over the range of n studied (except for the largest n values at small L and in the small n limit). Straight lines are obtained when we assume an underlying Gaussian distribution of percolation thresholds (i.e., $a=2$), although due to the small exponent ($\beta/2 \approx 0.2$) it is difficult to predict a accurately. Note that a log-log plot of X versus $\ln n$ cannot be used to determine the appropriate exponent due to the presence of a nonzero constant in Eq. (2.32). Comparing the

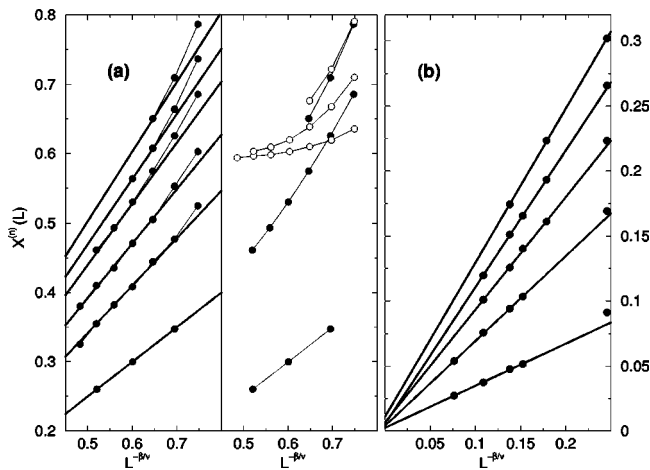


FIG. 10. L -dependent scaling of the density of EL's. Points represent numerical results. (a) $D=2$. In the left panel EL's of size $n=1, 2, 4, 16, 64$, and 1000 are given from bottom to top. Thick lines represent linear fits to the large L range of the data, indicating scaling according to Eq. (2.32). In the right panel results for $n=2, 16$, and 1000 are compared to the percolation thresholds (open circles), indicating scaling according to Eq. (2.33). (b) $D=3$, $n=1, 2, 4, 10$, and 50 from bottom to top. Thick lines represent linear fits to all but the smallest L value, indicating scaling according to Eq. (2.32).

density to the percolation thresholds, Fig. 11(b) shows that, even for the smallest L value studied, the next anticipated scaling regime [Eq. (2.34)] is not yet reached in 3D. In 2D [Fig. 11(a), left panel] the situation is different. Scaling according to Eq. (2.32) is observed but with an exponent of β/ν instead of $\beta/2$ in accordance with the observed scaling of the percolation threshold. For larger n the next scaling regime is entered [Fig. 11(a), right panel], and the limiting curves that scale according to Eq. (2.33) start coinciding with the density curves.

IV. CONCLUSION

Statistical arguments show that the percolation threshold of a lattice that is elongated in one direction is shifted towards higher values. The shift in percolation threshold with respect to the simple lattice (SL) was derived to scale as approximately $\ln n^{1/a}$, with n being the aspect ratio of the lattice and a being the appropriate exponent of the percolation probability distribution of the SL. The scaling with lat-

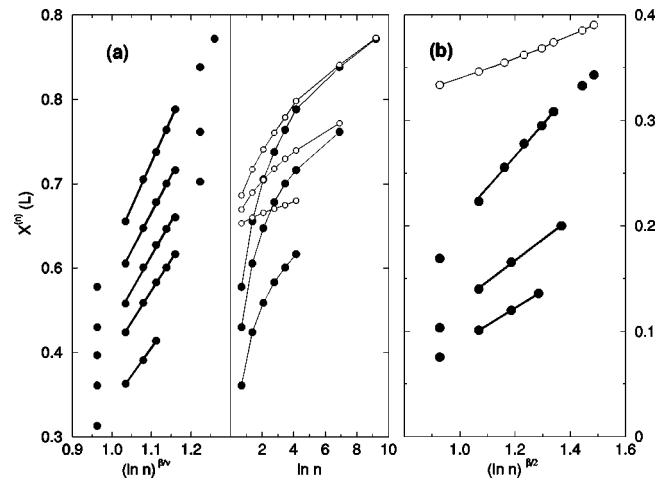


FIG. 11. n -dependent scaling of the density of EL's. (a) $D=2$. In left panel filled circles are numerical data for EL's of size $L=16, 32, 64, 128$, and 512 from top to bottom. The thick lines represent linear fits to intermediate values of n . The right panel shows the same data plus the observed percolation thresholds (open circles) for $L=16, 32$, and 128 . (b) $D=3$. $L=16, 41$, and 80 from top to bottom. Open circles denote the percolation threshold in case of $L=16$.

tice size L is shown to be identical to that of a SL. Both scaling laws apply in 2D and 3D. Numerical results over wide ranges of n and L confirm the theoretically-derived scaling relationships. For the density of the percolating cluster two different scaling laws are derived. Numerical results indicate that one of them, in which the percolation threshold is still close to that of the SL, applies partly to the 2D, and fully to the 3D case. The critical exponent β of random percolation appears in the scaling relations. The other regime, in which the percolation threshold has shifted substantially away from that of the SL is reached in 2D. In this case the density of the percolating cluster and the percolation threshold become almost identical, i.e., almost all the occupied sites are in the percolating cluster.

ACKNOWLEDGMENTS

M.A.K. is grateful to the Australian Research Council for financial support. We thank the ANU Supercomputing Facility for generous allocations of computer time. M.A.K. acknowledges discussions with K. Mecke, M. Sahimi, and D. Stauffer.

-
- [1] D. Stauffer and A. Aharony, *Introduction to Percolation Theory*, 2nd ed. (Taylor and Francis, London, 1994).
 - [2] M. Sahimi, *Applications of Percolation Theory*, 1st ed. (Taylor and Francis, London, 1994).
 - [3] M. Sahimi, *Rev. Mod. Phys.* **65**, 1393 (1993).
 - [4] M. Sahimi, *Phys. Rep.* **306**, 213 (1998).
 - [5] R. A. Monetti and E. V. Albano, *Z. Phys. B: Condens. Matter* **82**, 129 (1991).
 - [6] R. A. Monetti and E. V. Albano, *Z. Phys. B: Condens. Matter* **90**, 351 (1993).
 - [7] J. L. Cardy, *J. Phys. A* **17**, L961 (1984).
 - [8] R. P. Langlands, C. Pichet, P. Pouliot, and Y. S. Aubin, *J. Stat. Phys.* **67**, 553 (1992).
 - [9] C. D. Lorenz and R. M. Ziff, *J. Phys. A* **31**, 8147 (1998).
 - [10] M. Honarpour, L. Koederitz, and A. H. Harvey, *Relative Permeability of Petroleum Reservoirs* (CRC Press, Boca Raton, FL, 1986).
 - [11] R. Larson, L. E. Scriven, and H. T. Davis, *Nature (London)* **268**, 409 (1977).
 - [12] S. J. Marrink and M. A. Knackstedt, *J. Phys. A* **32**, L461 (1999).
 - [13] P. J. Reynolds, H. E. Stanley, and W. Klein, *Phys. Rev. B* **21**,

- 1223 (1980).
- [14] J. Vannimenus and J. P. Nadal, Phys. Rep. **103**, 47 (1984).
- [15] R. M. Ziff, Phys. Rev. Lett. **72**, 1942 (1994).
- [16] U. Haas, Physica A **215**, 247 (1995).
- [17] L. Beryland and J. Wehr, J. Phys. A **28**, 7127 (1995).
- [18] J. Cardy, J. Phys. A **31**, L105 (1998).
- [19] J. L. Cardy, J. Phys. A **25**, L201 (1992).
- [20] R. M. Ziff, Phys. Rev. E **54**, 2547 (1996).
- [21] R. M. Ziff, Phys. Rev. Lett. **69**, 2670 (1992).
- [22] J.-P. Hovi and A. Aharony, Phys. Rev. E **53**, 235 (1996).
- [23] J. C. Gimel, T. Nicolai, and D. Durand, J. Phys. A **32**, L515 (1999).
- [24] C. Y. Lin, C. K. Hu, and J.-A. Chen, J. Phys. A **31**, L111 (1998).
- [25] M. Acharyya and D. Stauffer, Int. J. Mod. Phys. C **9**, 643 (1998).